

## *Retraction*

# **Retracted: Dynamic Response of a Semiactive Suspension System with Hysteretic Nonlinear Energy Sink Based on Random Excitation by means of Computer Simulation**

### **Complexity**

Received 19 December 2023; Accepted 19 December 2023; Published 20 December 2023

Copyright © 2023 Complexity. This is an open access article distributed under the Creative Commons Attribution License, which permits unrestricted use, distribution, and reproduction in any medium, provided the original work is properly cited.

This article has been retracted by Hindawi following an investigation undertaken by the publisher [1]. This investigation has uncovered evidence of one or more of the following indicators of systematic manipulation of the publication process:

- (1) Discrepancies in scope
- (2) Discrepancies in the description of the research reported
- (3) Discrepancies between the availability of data and the research described
- (4) Inappropriate citations
- (5) Incoherent, meaningless and/or irrelevant content included in the article
- (6) Manipulated or compromised peer review

The presence of these indicators undermines our confidence in the integrity of the article's content and we cannot, therefore, vouch for its reliability. Please note that this notice is intended solely to alert readers that the content of this article is unreliable. We have not investigated whether authors were aware of or involved in the systematic manipulation of the publication process.

Wiley and Hindawi regrets that the usual quality checks did not identify these issues before publication and have since put additional measures in place to safeguard research integrity.

We wish to credit our own Research Integrity and Research Publishing teams and anonymous and named external researchers and research integrity experts for contributing to this investigation.

The corresponding author, as the representative of all authors, has been given the opportunity to register their agreement or disagreement to this retraction. We have kept a record of any response received.

### **References**

- [1] H. Chen and W. Jin, "Dynamic Response of a Semiactive Suspension System with Hysteretic Nonlinear Energy Sink Based on Random Excitation by means of Computer Simulation," *Complexity*, vol. 2020, Article ID 3181423, 13 pages, 2020.

## Research Article

# Dynamic Response of a Semiactive Suspension System with Hysteretic Nonlinear Energy Sink Based on Random Excitation by means of Computer Simulation

Hui Chen  and Wuyin Jin 

School of Mechanical & Electromechanical Engineering, Lanzhou University of Technology, Lanzhou 730050, China

Correspondence should be addressed to Wuyin Jin; wuyinjin@hotmail.com

Received 12 July 2020; Revised 18 August 2020; Accepted 26 August 2020; Published 17 September 2020

Academic Editor: Zhihan Lv

Copyright © 2020 Hui Chen and Wuyin Jin. This is an open access article distributed under the Creative Commons Attribution License, which permits unrestricted use, distribution, and reproduction in any medium, provided the original work is properly cited.

This paper aims to investigate the property and behavior of the hysteretic nonlinear energy sink (HNES) coupled to a half vehicle system which is a nine-degree-of-freedom, nonlinear, and semiactive suspension system in order to improve the ride comfort and increase the stability in shock mitigation by using the computer simulation method. The HNES model is a semiactive suspension device, which comprises the famous Bouc–Wen (B-W) model employed to describe the force produced by both the purely hysteretic spring and linear elastic spring of potentially negative stiffness connected in parallel, for the half vehicle system. Nine nonlinear motion equations of the half vehicle system are derived in terms of the seven displacements and the two dimensionless hysteretic variables, which are integrated numerically by employing the direct time integration method for studying both the variables of vertical displacements, velocities, accelerations, chassis pitch angle, and the ride comfort and driver safety, respectively, based on the bump and random road inputs of the pseudoexcitation method as excitation signal. Simulation results show that, compared with the HNES model and the magnetorheological (MR) model coupled to the half vehicle system, the ride comfort and stability have been evidently improved. A successful validation process has been performed, which indicated that both the ride comfort and driver safety properties of the HNES model coupled to half vehicle significantly improved.

## 1. Introduction

To achieve both ride comfort and driver safety is the main objective of the vehicle industry, and there are two ways to achieve ride comfort of high quality; to this end, the first way is to minimize the axis and angular acceleration of the gravity center of the vehicle body, while the second way is to maintain the tire contacts with the ground while the tire strikes a bump. Minimizing the vertical displacement of the vehicle can facilitate the ride stability.

Passive, active, and semiactive suspension vehicle systems are three available classifications of suspensions which depend on the ability of the suspension system to absorb, add, or extract energy. More recently, one of the oldest passive vibration control devices is the tuned mass damper (TMD) which was proposed by Watts in 1883 [1] and patented by Frahm [2], consisting of a mass, a spring, and a viscous

damper which is attached to a primary vibrating system in order to suppress undesirable vibrations. The property of the TMD can be significantly reduced for the environmental influences, and other external parameters may alter its properties and disturb its tuning [3]. To help reduce the vibration, a large oscillating mass is generally required. Both construction and placement are rather difficult. In light of the above drawbacks, to overcome the disadvantages of the TMD, new nonlinear strategies in vibration absorption have been introduced, and among them, researchers investigated the targeted energy transfer (TET) through different designs of NES, so they have gained more attention and are more prevalent [4]. According to [5], definitely, the NES is a nonlinear attachment coupled to a linear system which dissipates energy irreversibly through nonlinear stiffness elements. To help dissipate energy effectively, compared with the TMD, the NES does not need to be tuned to a special

frequency. The performance of nonsmooth NES in the presence of gravity has also been investigated where the pure cubic nonlinearity is broken in vertical configurations as the gravity induces asymmetry to the system [6, 7].

The concept of hysteretic nonlinear energy sink (HNES) was proposed by Tsiatas and studied by Tsiatas and Charalampakis in 2018 [8]. The HNES is the modification of the NES [9, 10], i.e., apart from a small mass and a nonlinear elastic spring of the duffing oscillator, the HNES also comprises a purely hysteretic spring and a linear elastic spring of potentially negative stiffness, connected in parallel. The BoucWen (B-W) model is used to describe the force produced by the purely hysteretic and linear elastic springs and has been investigated in NES dynamics previously [11, 12].

Eltantawie has studied the mechanical behavior of the magnetorheological damper (MRD) as a semiactive device of the vehicle suspension system for decentralized neurofuzzy control method previously. In this paper, the HNES model is employed as a semiactive suspension device and coupled to the linear half vehicle system in order to improve the ride comfort and increase the stability.

This study proposes a comprehensive design by using the HNES model as the semiactive suspension device, and the motion equations of the vehicle system which consist of the HNES model have been established, followed by employing the new direct time integration method, which is presented for solution of motion equations describing the dynamic response of multi-degree-of-freedom, structural linear and nonlinear systems in 2014 [13], for the solution of the system of first-order ordinary differential equations which represent semidiscrete diffusion equations in 2016 [14], and for solution of the motion equations of the vehicle model by means of the computer simulation method.

The rest of this paper is organized as follows: Section 2 describes and analyzes both half vehicle system and the HNES coupled to a primary model. The differential equations of the HNES coupled to a primary model and the semiactive suspension system are analyzed by employing the new direct time integral method, which be formulated in Section 3. The responses of the displacements, velocity, acceleration, and chassis pitch angle in the time domain are simulated by the parameters of half vehicle system in Section 4. The ride comfort and drive safety of half vehicle system are solved numerically, which are described in the Section 5. The main conclusions and findings are drawn in Section 6.

## 2. Half Vehicle and the HNES Model

**2.1. Half Vehicle Coupling with the HNES Model.** In this paper, a semiactive suspension system of the half vehicle model, which consists of sprung mass supported on front and rear suspensions as shown in Figure 1, is proposed. Both the front and rear suspensions which are considered as unsprung masses with the front and rear tire mass are connected to their tire axles, respectively. Damper  $C_f$ , elastic device  $K_f$  and HNES model (details of the HNES model is described in Section 2.2) are connected through chassis mass  $M_2$  and front tire directly in parallel, same as the front suspension, damper

$C_r$ , elastic device  $K_r$  and HNES model connected through chassis mass  $M_2$  and rear tire in parallel. The model is a nine-degree-of-freedom system and represented by the displacements of vertical driver  $U_5$ , vertical vehicle body  $U_4$ , body pitch  $U_3$ , front and rear tire deflections  $U_{f1}$  and  $U_{r1}$  and  $U_{f2}$  and  $U_{r2}$  of the mass  $M_1$ , and the displacements  $U_{Zf}$  and  $U_{Zr}$  which indicates the BoucWen model (Figure 1).

The mathematical model is derived by applying Newton's second law; the motion equations can be formulated as follows:

$$M_3\ddot{U}_5 + C_{f2}(\dot{U}_5 - (\dot{U}_4 - \dot{U}_3L_3)) + K_{f2}(U_5 - (U_4 - U_3L_3)) = 0, \quad (1)$$

$$\begin{aligned} M_2\ddot{U}_4 - C_{f2}(U_5 - (\dot{U}_4 - \dot{U}_3L_3)) - K_{f2}(U_5 - (U_4 - U_3L_3)) \\ + K_f(U_4 - U_3L_1 - U_{f1}) + C_f(\dot{U}_4 - \dot{U}_3L_1 - \dot{U}_{f1}) \\ + C_2(\dot{U}_4 - \dot{U}_{f2} - \dot{U}_3L_1) + K_{NL}(U_4 - U_{f2} - U_3L_1)^3 \\ + K_r(U_4 - U_{r1} + U_3L_2) + C_r(\dot{U}_4 - \dot{U}_{r1} + \dot{U}_3L_1) \\ + C_2(\dot{U}_4 - \dot{U}_{r2} + \dot{U}_3L_2) + K_{NL}(U_4 - U_{r2} + U_3L_2) \\ = -F_{BWf} - F_{BWr}, \end{aligned} \quad (2)$$

$$\begin{aligned} M_1\ddot{U}_{f2} - C_2(\dot{U}_4 - \dot{U}_{f2} - \dot{U}_3L_1) - K_{NL}(U_4 - U_{f2} - U_3L_1)^3 \\ + C_1(\dot{U}_{f2} - \dot{U}_{f1}) + K_{EL}(U_{f2} - U_{f1}) = F_{BWf}, \end{aligned} \quad (3)$$

$$\begin{aligned} M_1\ddot{U}_{r2} - C_2(\dot{U}_4 - \dot{U}_{r2} + \dot{U}_3L_2) - K_{NL}(U_4 - U_{r2} + U_3L_2)^3 \\ + C_1(\dot{U}_{r2} - \dot{U}_{r1}) + K_{EL}(U_{r2} - U_{r1}) = F_{BWr}, \end{aligned} \quad (4)$$

$$\begin{aligned} M_f\ddot{U}_{f1} - K_f(U_4 - U_{f1} - U_3L_1) - C_f(\dot{U}_4 - \dot{U}_{f1} - \dot{U}_3L_1) \\ - C_1(\dot{U}_{f2} - \dot{U}_{f2}) - K_{EL}(U_{f2} - U_{f1}) + K_{tr}(U_{f1} - q_1) = 0, \end{aligned} \quad (5)$$

$$\begin{aligned} M_r\ddot{U}_{r1} - K_r(U_4 - U_{r1} + U_3L_2) - C_r(\dot{U}_4 - \dot{U}_{r1} + \dot{U}_3L_2) \\ - C_1(\dot{U}_{r2} - \dot{U}_{r1}) - K_{EL}(U_{r2} - U_{r1}) + K_{tr}(U_{r1} - q_2) = 0, \end{aligned} \quad (6)$$

$$\begin{aligned} J\ddot{U}_3 + C_{f2}(\dot{U}_5 - (\dot{U}_4 - L_3\dot{U}_3))L_3 + K_{f2} \\ \cdot (U_5 - (U_4 - L_3U_3))L_3 - K_f((U_4 - L_1U_3) - U_{f1})L_1 \\ - C_f((\dot{U}_4 - L_1\dot{U}_3) - \dot{U}_{f1})L_1 \\ - C_2((\dot{U}_4 - L_1\dot{U}_3) - \dot{U}_{f2})L_1 - K_{NL} \\ \cdot ((U_4 - L_1U_3) - U_{f2})^3L_1 + K_r((U_4 + L_2U_3) - U_{r1})L_2 \\ + C_r((\dot{U}_4 + L_2\dot{U}_3) - \dot{U}_{r1})L_2 + C_2 \\ \cdot ((\dot{U}_4 + L_2\dot{U}_3) - \dot{U}_{r2})L_2 + K_{NL}((U_4 + L_2U_3) - U_{r2})^3L_2 \\ = -F_{BWf}L_1 - F_{BWr}L_2, \end{aligned} \quad (7)$$



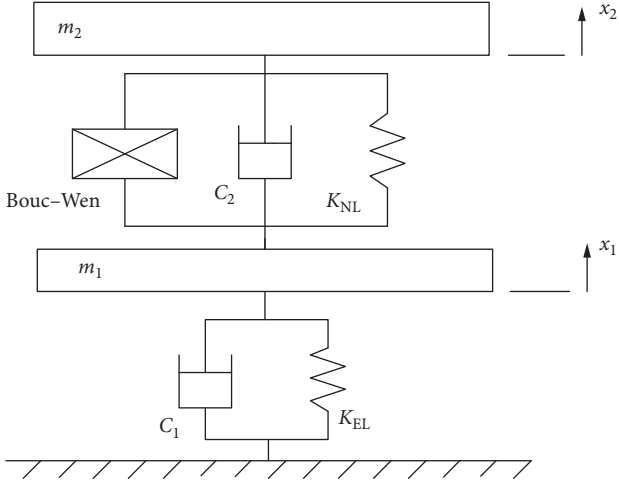


FIGURE 2: The SDof primary system coupling with HNES (the HNES model).

where  $n > 0$ ,  $\text{sgn}(\cdot)$  denotes the signum function,  $x$  is the displacement,  $k$  is the initial stiffness,  $\alpha$  is the ratio of postyield to preyield stiffness,  $D$  indicates the yield displacement, the dimensionless exponential parameter  $n$  governs the abruptness of transition between preyield and postyield response, and the values of  $\alpha$ ,  $A$ ,  $\beta$ ,  $D$ ,  $\gamma$ , and  $n$  are set in Table 1 [8].

The HNES model is derived by applying Newton's second law, and the equations of motion can be formulated as follows:

$$m_1 \ddot{x}_1 + C_2 \dot{x}_1 + K_{EL} x_1 - F_{BW} - C_2 (\dot{x}_2 - \dot{x}_1) - K_{NL} (x_2 - x_1)^3 = 0, \quad (15)$$

$$m_2 \ddot{x}_2 + F_{BW} + C_2 (\dot{x}_2 - \dot{x}_1) + K_{NL} (x_2 - x_1)^3 = 0, \quad (16)$$

$$\dot{z}(t) = D^{-1} (\dot{x}_2 - \dot{x}_1) (1 - |z(t)|^n (\text{sgn}(\dot{x}_2 - \dot{x}_1) z(t)) + b). \quad (17)$$

In this investigation, only the direct impulsive force of the primary system is considered, and thus, the initial conditions of the problem are as follows:

$$\begin{aligned} \dot{x}_1(0) &= v_0, \\ x_1(0) = \dot{x}_2(0) = \dot{x}_2(0) &= 0, \end{aligned} \quad (18)$$

where  $m_1$ ,  $x_1$ ,  $K_{EL}$ , and  $C_1$  are the mass, displacement, stiffness of spring, and damping coefficient of the linear primary system, respectively, and  $m_2$ ,  $x_2$ ,  $K_{NL}$ , and  $C_2$  are the mass, displacement, damping coefficient, and cubic nonlinear stiffness of the HNES's attachments.

### 3. State Space Form of the Motion Equations and the Excitation of Road Inputs

**3.1. State Space Form.** Equations (15)–(18) can be reorganized into state space form as follows:

TABLE 1: Parameters of HNES (dimensionless).

Parameter	$\alpha$	$A$	$\beta$	$D$	$\gamma$	$n$
Value	-0.3	1	0.5	0.1	0.5	1

$$\{\mathbf{X}_n\} = \begin{cases} X_1 = x_1 \\ X_2 = \dot{x}_1 \\ X_3 = x_2 \\ X_4 = \dot{x}_2 \\ X_5 = z(t) \end{cases}, \quad (19)$$

$$\begin{cases} \dot{X}_1 = X_2 \\ \dot{X}_2 = \frac{F_{BW} - C_1 X_2 - K_{EL} X_1 + C_2 (X_4 - X_2) + K_{NL} (X_2 - X_1)^3}{m_1} \\ \dot{X}_3 = X_4 \\ \dot{X}_4 = \frac{-F_{BW} - C_2 (X_4 - X_2) - K_{NL} (X_3 - X_1)^3}{m_2} \\ \dot{X}_5 = D^{-1} (X_4 - X_2) (1 - |X_5|^n (\gamma \text{sgn}(X_4 - X_2) X_2) + \beta) \end{cases}. \quad (20)$$

Together with the pertinent initial conditions, the following can be expressed:

$$\{\dot{X}_n(0)\} = \begin{cases} \dot{X}_1(0) = v_0 \\ \dot{X}_2(0) = \frac{(C_1 + C_2)v_0}{m_1} \\ \dot{X}_3(0) = \frac{C_2 v_0}{m_2} \\ \dot{X}_4(0) = \frac{C_2 v_0}{m_2} \\ \dot{X}_5(0) = \frac{v_0}{D} \end{cases}, \quad (21)$$

where  $v_0 = \dot{x}_1(0)$  denotes the initial value.

Equations (19)–(21) can be rewritten as follows:

$$\begin{aligned} \mathbf{M}_i^{-1} \mathbf{F}(t) - \mathbf{M}_i^{-1} \mathbf{P}(\mathbf{X}_n(t), \dot{\mathbf{X}}_n(t)) \\ = f(\mathbf{X}_n(t) + \mathbf{X}_n(t), t) = \mathbf{0}, \quad n = 1, 2, \dots, 5, \end{aligned} \quad (22)$$

where  $\mathbf{M}_i$ ,  $i = 1, 2$ , denotes the mass matrix which consists of  $m_1$  and  $m_2$  and function  $f(\mathbf{X}_n(t) + \mathbf{X}_n(t), t)$  is already expressed in equation (20).

It should be noteworthy that equation (22) is a typical nonlinear initial value problem, which are solved numerically using the new direct time integration method

introduced by Katsikadelis [13], and that for multidegree of freedom systems is described as follows:

$$\mathbf{X}_{n-k} = \dot{\mathbf{X}}_{n-k-1}(t) + \frac{h}{2}\dot{\mathbf{X}}_{n-k}(t) + \frac{h}{2}\dot{\mathbf{X}}_{n-k-1}(t), \quad (23)$$

where  $\mathbf{X}_{n-k}$  denotes the responses of the displacement vector, of which elements are the value in different time histories for  $k = 1, 2, \dots, (T/h)$ .  $T$  is the simulation period, and  $h$  is the sampling interval.  $\dot{\mathbf{X}}_{n-k}$  and  $\mathbf{X}_{n-k}$  can be solved by coupling equations (22) and (23) with  $k = 1, 2, \dots, T/h$ .

Figure 3 depicts the responses of displacements  $X_1$  and  $X_3$  of the masses  $m_1$  and  $m_2$  of primary system coupling with HNES against the impulse magnitude  $v_0$  for  $v_0 = 0.35$  m/s,  $h = 0.01$ , and  $T = 500$  seconds (Figure 3(a)) and  $v_0 = 2$  m/s,  $h = 0.01$ , and  $T = 500$  seconds (Figure 3(b)). It can be observed that displacements  $X_1$  and  $X_3$  against time are similar in shape during 500 seconds, and the amplitude changes more slowly over the entire time domain, and the maximum values of amplitudes are  $X_1 = 2.1$  m and  $X_2 = 2.3$  m (Figure 3(b)) and  $X_1 = 0.12$  m and  $X_3 = 0.01$  m (Figure 3(a)).

### 3.2. Excitation of Road Inputs

**3.2.1. Bump Road Inputs.** The bump road excitation method is one of the simple inputs for a vehicle, which has the equations as follows [19]:

$$q_i(t) = \begin{cases} \frac{u_r(1 - \cos(8\pi t))}{2}, & 0.5 \leq t \leq 0.75, \\ 0, & \text{otherwise,} \end{cases} \quad (24)$$

where  $i (=1, 2)$  represents the front and rear tire, respectively,  $u_r = 0.11$  m denotes the amplitude of bump road excitation, simulation period  $T = 4$  seconds, the bump road excitation for the rear tire is assumed to be that of the front but with a time delay (seconds) of  $\tau$ , and sampling interval  $h = 0.01$  seconds in this study. Time delay  $\tau$  is formulated as follows:

$$\tau = \frac{L_1 + L_2}{v}, \quad (25)$$

where symbol  $v$  denotes the vehicle velocity and  $L_1$  and  $L_2$  are the front and rear wheelbase; the excitation signals for bump road inputs are shown in Figure 4(a).

The road excitation of rear tire inputs  $q_2(t)$  is formulated as

$$q_2(t) = q_1(t - \tau). \quad (26)$$

**3.2.2. Random Excitation of Road Surface Roughness.** The road power spectral density (PSD) about the spatial frequency is  $G_q(n)$ ,  $n_1 < n < n_2$  ( $n = f/v$ ), where  $v$  is the average vehicle velocity and  $n$  is the spatial frequency. The road surface roughness variance of  $\sigma_q^2$  by using the frequency spectrum properties of average stationary random process can be expressed as follows [20]:

$$\sigma_q^2 = \int_{n_1}^{n_2} G_q(n) dn. \quad (27)$$

Dividing the area ( $n_1, n_2$ ) into  $m$  smaller intervals, the frequency of the power spectral density value is  $G_q(n_{\text{mid}-i})$  instead of  $G_q(n)$  at each small interval of the central part, where  $n_{\text{mid}-i}$ ,  $i = 1, 2, \dots, m$ . Throughout, the area between the value of the formula after discretization approximation can be written as follows:

$$\sigma_q^2 \approx \sum_{i=1}^m G_q(n_{\text{mid}-i}) \cdot \Delta n_i. \quad (28)$$

Corresponding to each small range, we need to find the frequency for  $n_{\text{mid}-i}$  ( $i = 1, 2, 3, \dots, m$ ) and the standard deviation of  $\sqrt{G_q(n_{\text{mid}-i}) \cdot \Delta n_i}$  sine wave function, and such sine wave function can be expressed as

$$\sqrt{G_q(n_{\text{mid}-i}) \cdot \Delta n_i} \cdot \sin(2\pi n_{\text{mid}-i} x + \theta_i). \quad (29)$$

Then, the corresponding sine wave function in each area is added up to obtain the road random displacement input on the time domain:

$$q_j(t) = \sqrt{2} \sum_{i=1}^m \sqrt{G_q(n_{\text{mid}-i}) \cdot \Delta n_i} \cdot \sin(2\pi n_{\text{mid}-i} t + \theta_i), \quad j = 1, 2, \quad (30)$$

where  $\theta_i$  is uniformly distributed random numbers between  $[-\pi, \pi]$ , of which probability density and distribution function can be referred to in Appendix B. And,  $t$  denotes the time history which can be normalized by  $s/v$  ( $s$  is the total distance traveled by the vehicle in this study). According to reference [21], the spatial frequency  $n$  of road is distributed between  $[0.011, 2.83] \text{ m}^{-1}$ . In this study, considering both the relevant regulations and practical life experience, the range of vehicle velocity  $V_v \in [V_{n-\min}, V_{n-\max}] = [10, 30] \text{ m/s}$  (36–108 km/h).

Relationships between time frequency  $f$  and spatial frequency  $n$  of the vehicle can be formulated as equation  $f = vn$  (Hz). Therefore, the range of road spatial frequency in this paper can be expressed as follows:

$$\begin{aligned} \mathbf{A}_n &= \mathbf{A}_{n1} \cap \mathbf{A}_{n2} = [V_{n-\min} \times 0.011, V_{n-\min} \times 2.83] \\ &\cap [V_{n-\max} \times 0.011, V_{n-\max} \times 2.83] = [0.33, 28.3]. \end{aligned} \quad (31)$$

Here,  $\mathbf{A}_{n1}$  and  $\mathbf{A}_{n2}$  denote the spatial frequency range at lowest velocity  $V_{n-\min}$  and at the highest velocity  $V_{n-\max}$  and symbol  $\cap$  denotes a mathematical operation for the intersection of two sets.

The random excitation signal of road surface roughness is shown in Figure 4(b).

## 4. Simulation Response in the Time Domain

Equations (1)–(11) can be altered into equation (12) which is a nonlinear equation and can be written using the direct time integration method numerically as follows:

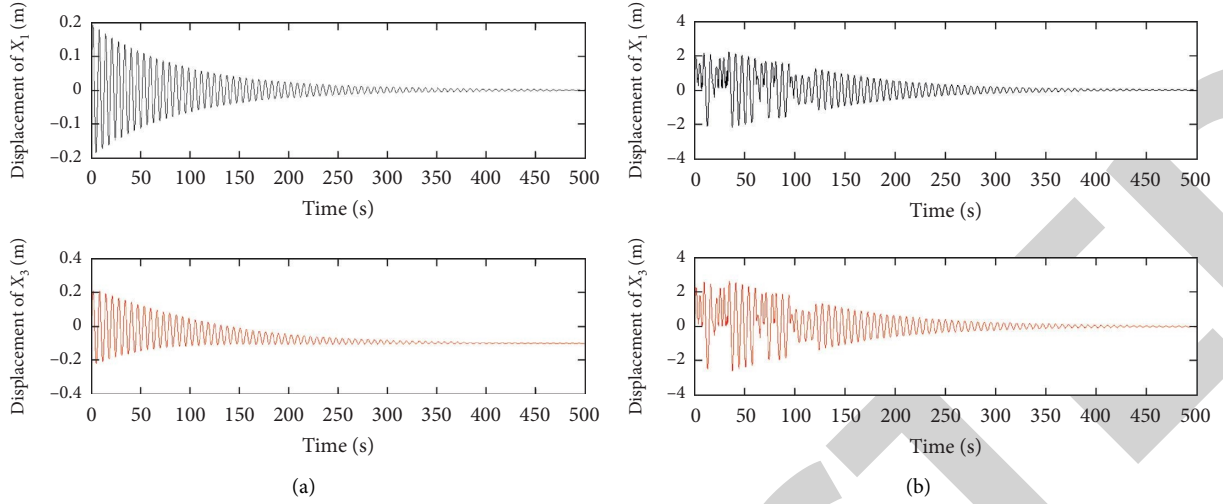


FIGURE 3: The response of displacements of the primary system coupling with the HNES model for  $v_0 = 0.35$  m/s,  $h = 0.01$ , and  $T = 500$  seconds (a) and  $v_0 = 2$  m/s,  $h = 0.01$ , and  $T = 500$  seconds (b).

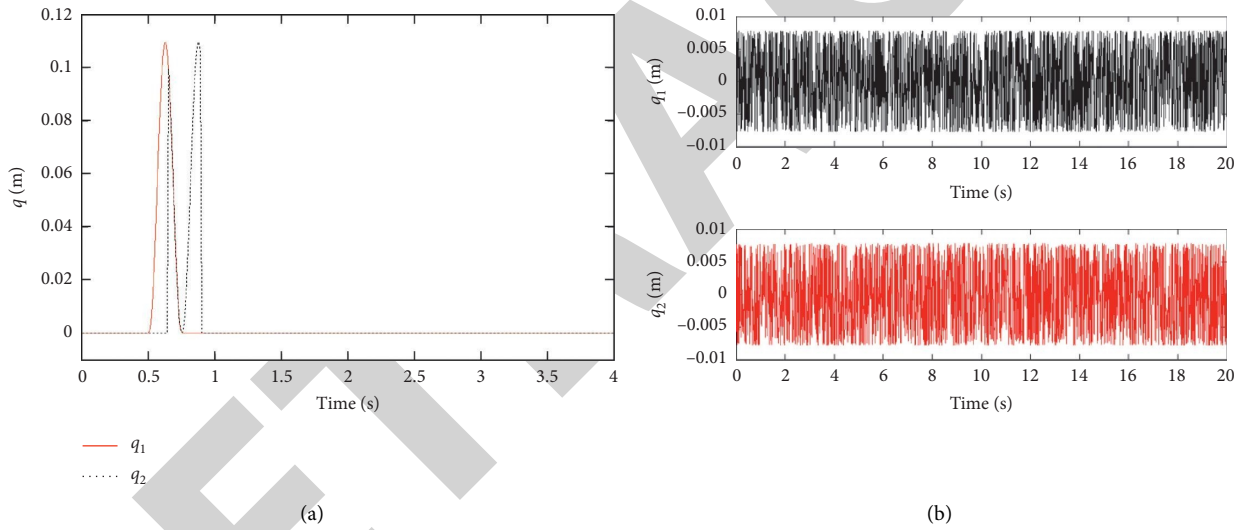


FIGURE 4: Two types of excitation signal for (a) the bump road inputs, where simulated period  $T = 4$  seconds, sampling interval  $h = 0.01$  second, and vehicle velocity  $v = 20$  m/s, and (b) the random road inputs, where simulated period  $T = 20$  seconds, sampling interval  $h = 0.01$  seconds, and vehicle velocity  $v = 20$  m/s.

$$\mathbf{M}\ddot{\mathbf{U}}_n + \mathbf{F}(\dot{\mathbf{U}}_n, \mathbf{U}_n) = \mathbf{P}_n, \quad (32)$$

$$\begin{bmatrix} -h\mathbf{I} & \mathbf{I} \\ \mathbf{I} & \mathbf{0} \end{bmatrix} \begin{Bmatrix} \dot{\mathbf{U}}_n \\ \mathbf{U}_n \end{Bmatrix} = \begin{bmatrix} \mathbf{0} & \mathbf{I} \\ \mathbf{I} & \mathbf{0} \end{bmatrix} \begin{Bmatrix} \dot{\mathbf{U}}_{n-1} \\ \mathbf{U}_{n-1} \end{Bmatrix} + \begin{bmatrix} \frac{\mathbf{r}_1}{2}\mathbf{I} \\ \frac{\mathbf{r}_2}{2}\mathbf{I} \end{bmatrix} \dot{\mathbf{U}}_n + \begin{bmatrix} \frac{\mathbf{r}_1}{2}\mathbf{I} \\ \frac{\mathbf{r}_2}{2}\mathbf{I} \end{bmatrix} \ddot{\mathbf{U}}_{n-1}, \quad (33)$$

$$\ddot{\mathbf{U}}_0 = \mathbf{M}^{-1}(\mathbf{P}_0 - \mathbf{F}(\dot{\mathbf{U}}_0, \mathbf{U}_0)), \mathbf{U}(0) = \mathbf{U}_0, \dot{\mathbf{U}}(0) = \dot{\mathbf{U}}_0, \quad (34)$$

$$\det(\mathbf{M}) \neq 0,$$

where  $r_1 = (h_2/2)$ ,  $r_2 = h$ ,  $h$  is the sampling interval time (second), and size  $(\mathbf{I}) = [9 \times 9]$  is the unit matrix.

$\ddot{\mathbf{U}}_n$ ,  $\dot{\mathbf{U}}_n$ , and  $\mathbf{U}_n$  can be solved by combining equations (32) and (33) with  $n = 1, 2, \dots, T/h$ .  $\dot{\mathbf{U}}_n$  and  $\mathbf{U}_n$  can be solved using equation (33) which is a linear equation and then substituting into equation (32) which is a nonlinear equation and can be solved to yield  $\dot{\mathbf{U}}_n$ . The function “fsovl” of *Matlab 2017a* has been employed to obtain the numerical results of both equations.

## 5. Performance Index and Numerical Simulation

**5.1. Response of Half Vehicle System Coupling with the HNES Model.** By querying the power spectral density coefficient (PSD) of standard road surface excitation  $G_q(n_0)$ [22] and referring a 10-degree-of-freedom (DOF) passenger vehicle model determine six state variables related to the longitudinal, lateral, and heave velocities and roll, pitch, and yaw rates [23]. Equations (32)–(34) can be solved using the software programming *Matlab 2017a* numerically. The parameters of half vehicle system coupling with the HNES model are given in Table 2.

Figure 5 depicts the response of vertical displacements of driver  $U_5$  and chassis  $U_4$  and pitch angle of chassis  $U_3$  against the road inputs for the bump excitation, of which simulation period  $T=10$  seconds, sampling interval  $h=0.01$ , and different velocities of the vehicle  $v=1.1256$  m/s (Figure 5(a)) and  $v=20$  m/s (Figure 5(b)), respectively. From these figures, it can be observed that for the bump road excitation with the amplitude  $A=0.11$  m, the chassis (sprung mass) reached a maximum of 0.05 m (Figure 5(a)) and 0.09 m (Figure 5(b)). Also when the inputs dropped to zero, the chassis (sprung mass) vertical displacement went down for only  $-0.001$  m (Figure 5(a)) and  $-0.01$  m (Figure 5(b)) which is almost zero. The overall amplitude achieved by the chassis is equal to that against the front and rear tire inputs. The response of the angular displacement of chassis had a maximum peak value of 0.021 rad (Figure 5(a)) and 0.04 rad (Figure 5(b)). However, when the rear tire of the vehicle received the input of road excitation, the maximum displacement response of the driver is  $-0.024$  m while the vehicle velocity is 1.1256 m/s, and  $-0.022$  m while the vehicle velocity is 20 m/s. Both values are smaller than the response values of the model in reference [24]. The output data obtained from Figure 5(a) for the maximum displacement of the vehicle body against time is 0.036 m, and the maximum angular displacement of the vehicle pitch angle is 0.02 rad which is smaller than of the model mentioned in reference [24].

The solution data obtained from the programs of the motion equations of the half vehicle system for velocity of the drive  $V_5$ , chassis (sprung mass)  $V_4$ , and angular velocity of the chassis  $V_3$  are plotted against time in Figure 6. It can be grasped that for bump excitation road inputs, the peak value is 0.11 m, simulation period  $T=10$  seconds, sampling interval  $h=0.01$  seconds, and different velocities of the vehicle  $v=1.1256$  m/s (Figure 6(a)) and  $v=20$  m/s (Figure 6(b)), respectively. When the front tire of the vehicle passed road excitation  $q^1(t)$ , the maximum velocity responses of the vehicle body are 0.21 m/s (a) and 0.272 m/s (b), respectively. When the rear tire excitation  $q^2(t)$  received by the vehicle gradually approaches 0 m, the velocity of the vehicle body only decreases by  $-0.08$  m/s (a) and  $-0.18$  m/s (b). These two values gradually tend to be stable after 10 seconds. The response of the driver velocity  $V_5$  stabilizes faster than others.

The responses of the displacements  $U_5, U_4$ , and  $U_3$ , velocities  $V_5, V_4$ , and  $V_3$ , and the accelerations  $A_5, A_4$ , and  $A_3$  against the road inputs were recorded for both the front and rear tire random excitation road inputs in Figures 7–9. It is obvious that the amplitude of displacement, velocity, and acceleration against time for the vehicle

TABLE 2: Main parameters of half vehicle system coupling with the HNES model.

Parameter	Meaning of the symbols	Value and units
$M_3$	Driver mass	65 kg
$M_2$	Chassis mass	708 kg
$M_f, M_r$	Front/rear unsprung mass	80 kg
$J$	Chassis inertia	2700 kg·m <sup>2</sup>
$L_1$	Horizontal distance from chassis mass center to the front axle	1.011 m
$L_2$	Horizontal distance from chassis mass center to the rear axle	1.803 m
$L_3$	Horizontal distance from chassis mass center to the driver	0.779 m
$U_5$	Driver vertical displacement	m
$U_4$	Chassis vertical displacement	m
$U_3$	Chassis pitching angle	rad
$U_f, U_r$	Vertical displacement of the front and rear axis	m
$K_{j2}$	Stiffness of connecting the chassis to the driver	23071 N/m
$K_f, K_r$	Stiffness of connecting chassis to the front and rear axle	1600 N/m
$K_{f\beta}, K_{r\beta}$	Stiffness of the front and rear tire	16000 N/m
$C_{t2}$	Damping coefficient connecting the chassis and driver	1500 N·s/m
$C_f, C_r$	Damping coefficient connecting chassis to front and rear axle	980 N·s/m
$C_1$	Damping coefficient of the linear primary system	0.001 N·s/m
$C_2$	Damping coefficient of the HNES attachments	0.01 N·s/m
$m_1$	Mass of the linear primary system	1 kg
$F_{BWf}, F_{BW_r}$	Force of the hysteretic restoring of the front/rear tire axle	N
$K_{NL}$	Cubic nonlinear stiffness of the HNES attachment	1 N/m <sup>3</sup>
$K_{EL}$	Stiffness of the linear primary system	1 N/m
$U_{j2}, U_{r2}$	Front and rear tire displacements of the linear primary system	m

velocity in Figure 7(a), Figure 8(a), and Figure 9(a) is smaller than that in Figure 7(b), Figure 8(b), and Figure 9(b), respectively. It can be seen that the displacement of vehicle body had a series random value, of which the maximum is 0.51 m, against the time for road inputs of random excitation, while the velocity of the vehicle is 20 m/s. It can be observed that the response of the displacement, velocity, and the acceleration of half vehicle system coupling with the HNES model against the road inputs for random excitation is very consistent with the vehicle theory, while the velocity is in the range [1.1256, 20] m/s. Therefore, from the dynamic response analysis, it can be known that it is reasonable and reliable to apply the HNES model to the vehicle system.

**5.2. Performance of the Half Vehicle System Coupling with the HNES Model.** Another simulation program has created with the aid of the semiactive suspension of half vehicle system coupling with the HNES model to obtain the drive safety and the ride comfort property. The drive safety and the quality of the contact between the tire and the road are described by

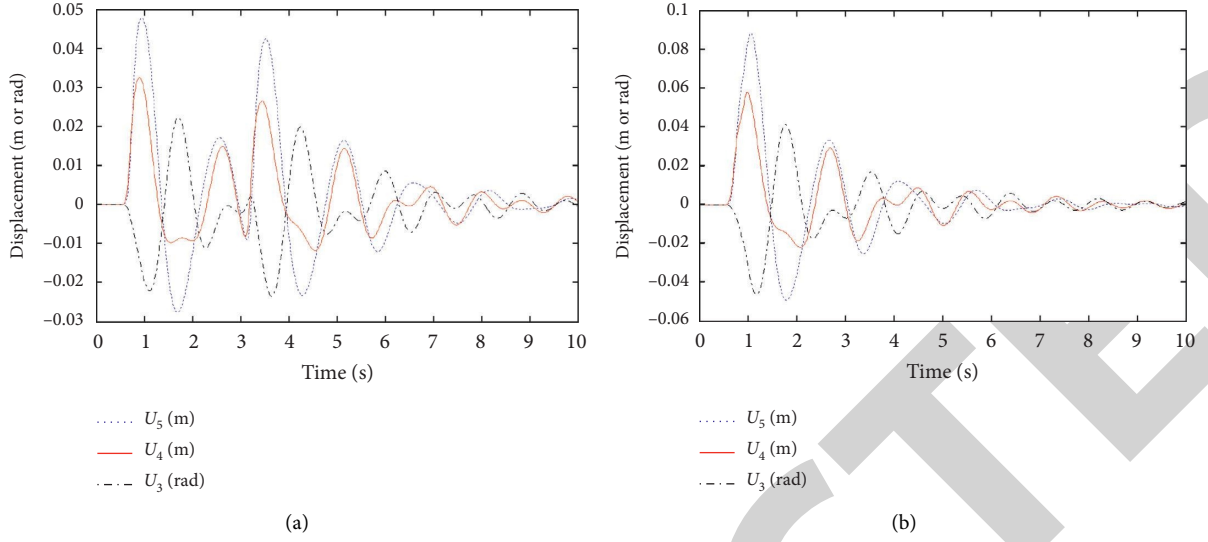


FIGURE 5: Responses of displacement  $\mathbf{U}_n$  of the half vehicle system while the excitation is bump road inputs. The vector  $\mathbf{U}_n$  represents the displacements of the driver  $U_5$ , the chassis  $U_4$ , and the pitch angle  $U_3$ , i.e.,  $\mathbf{U}_n = (U_5, U_4, U_3)^T$ , respectively. Simulation period  $T=10$  seconds, sampling interval  $h=0.01$  seconds, vehicle velocity  $v=1.1256$  m/s (the time delay  $\tau=2.5$  s) and (b) same as (a) except for the vehicle velocity  $v=20$  m/s (the time delay  $\tau=0.0938$  s).

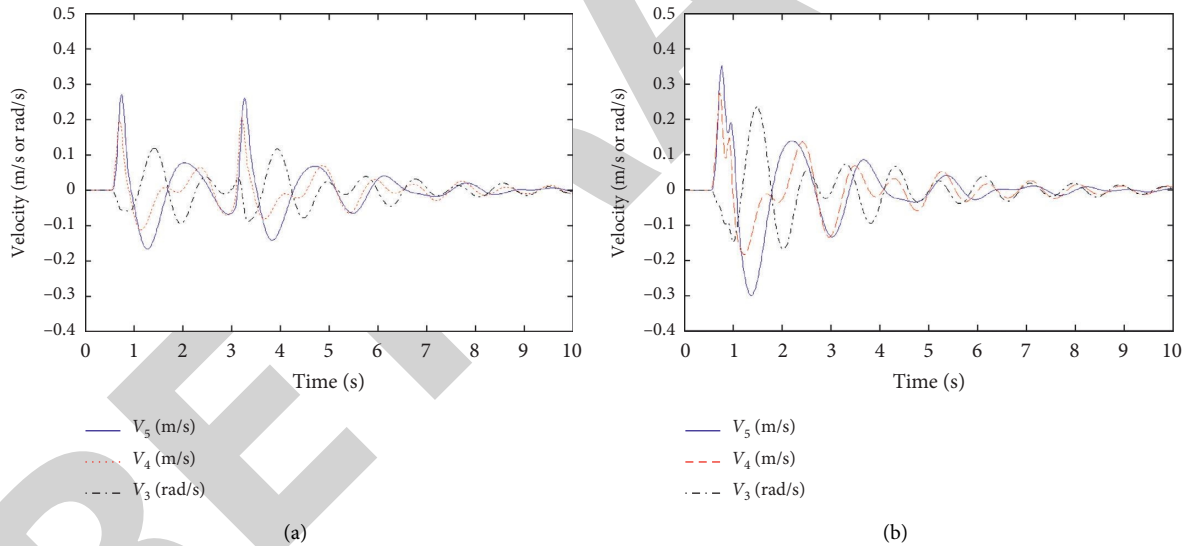


FIGURE 6: Responses of velocities  $\dot{\mathbf{U}}_n$  of half vehicle system coupling with the HNES model while excitation is bump road inputs and the velocity of vehicle is 1.1256 m/s (a) and 20 m/s (b). The vector  $\dot{\mathbf{U}}_n$  presents the velocities of the driver, the chassis, and the pitch angle.

the RMS (root mean square) value of the forces, which are dynamically exchanged by the tire and the road that is defined in [21]:

$$F_{U_{i1}D_{\text{dyn}}} = K_{\text{ti}}(U_{i1} - q_j). \quad (35)$$

Ride comfort can be formulated as

$$\ddot{U}_4^{\text{RMS}} = \sqrt{\frac{1}{T} \int_0^T \left( \frac{\ddot{U}}{g} \right)^2 dt}. \quad (36)$$

Drive safety can be formulated as

$$F_{U_{i1}, \text{dyn}}^{\text{RMS}} = \sqrt{\frac{1}{T} \int_0^T \left( \frac{F_{U_{i1}, \text{dyn}}}{F_{U_{i1}, \text{stat}}} \right)^2 dt}. \quad (37)$$

The steady-state load on the tire can be formulated as

$$F_{U_{i1}, \text{stat}} = (M_1 + M_i + M_2)g, \quad (38)$$

where  $i$  represents the front and rear suspensions, respectively, and  $j=1, 2$ .

Figure 10 shows the ratio of dynamic loads to static loads for the front (rear) tire, and the square of the ratio of

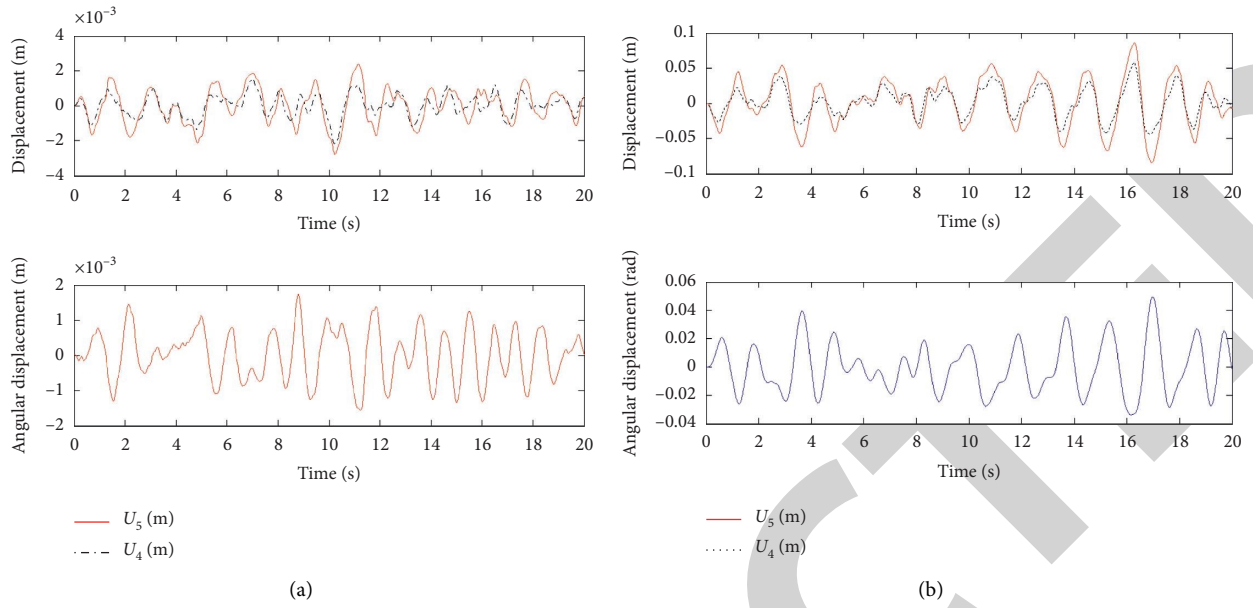


FIGURE 7: Responses of displacements  $U_n$  of half vehicle system coupling with the HNES model while the excitation is random road inputs and the velocity of vehicle is 1.1256 m/s (a) and 20 m/s (b).

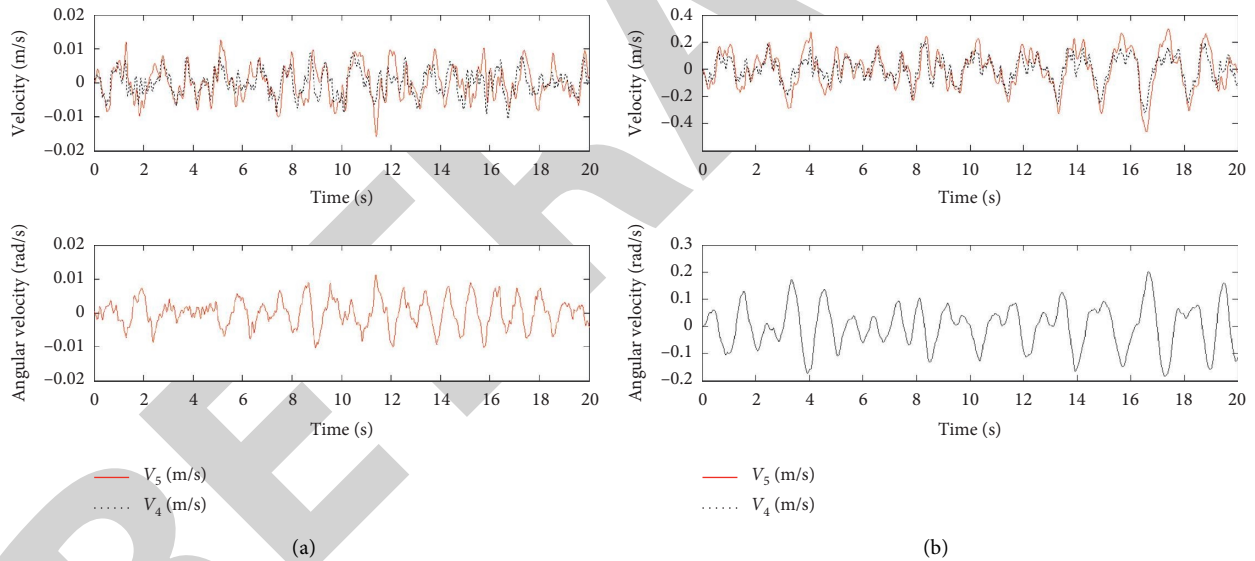


FIGURE 8: Responses of velocities  $V_n$  of half vehicle system coupling with the HNES model while the excitation is random road inputs and the velocity of vehicle is 1.1256 m/s (a) and 20 m/s (b).

acceleration to gravity acceleration  $g$  against the road inputs is recorded for bump road excitation in Figure 10(a) and road inputs for random excitation in Figure 10(b) while the vehicle velocity  $v = 1.1256$  m/s (the delay time is 2.5 seconds). It is obvious that the ratio of dynamic loads to static loads of the front tire had a maximum peak value of 0.48 against the road inputs for bump excitation in the time range of [0.5, 0.75] seconds, of which rear tire had a maximum peak value of 0.058 after the time delay of 2.5 seconds in Figure 10(a). The square of ratio of acceleration to gravity acceleration against the road inputs for bump excitation had a maximum peak value of 0.041 in the time range of [0.7, 0.75] seconds.

The maximum peak value of 0.58 was reached after the delay time of 2.5 seconds in Figure 10(a). The ratio of dynamic loads to static loads of the front (rear) tire, and the square of the ratio of acceleration to gravity acceleration against the road inputs for random excitation is very small which tends to zero as shown in Figure 10(b).

It can be observed from Tables 3 and 4 that the responses of displacements, velocities, and accelerations of the half vehicle system coupling with the HNES model are smaller. The ride comfort and driver safety properties are lower than those in the semiactive suspension of the MR model with the same parameters. However, ride comfort

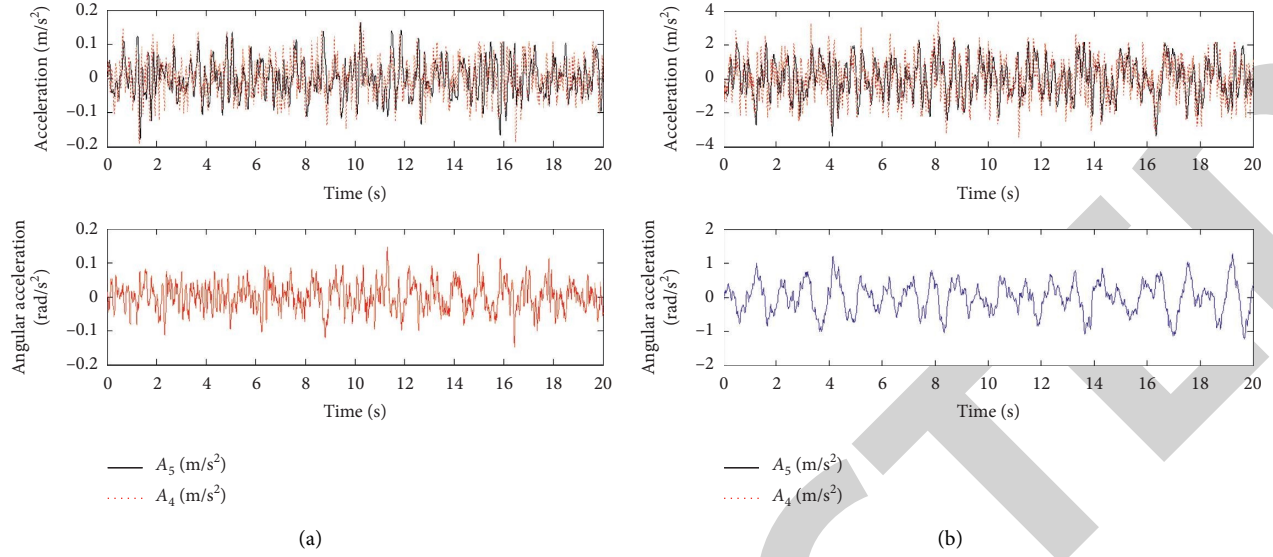


FIGURE 9: Responses of accelerations  $A_n$  of half vehicle system coupling with the HNES model while the excitation is random road inputs and the velocity of vehicle is 1.1256 m/s (a) and 20 m/s (b).

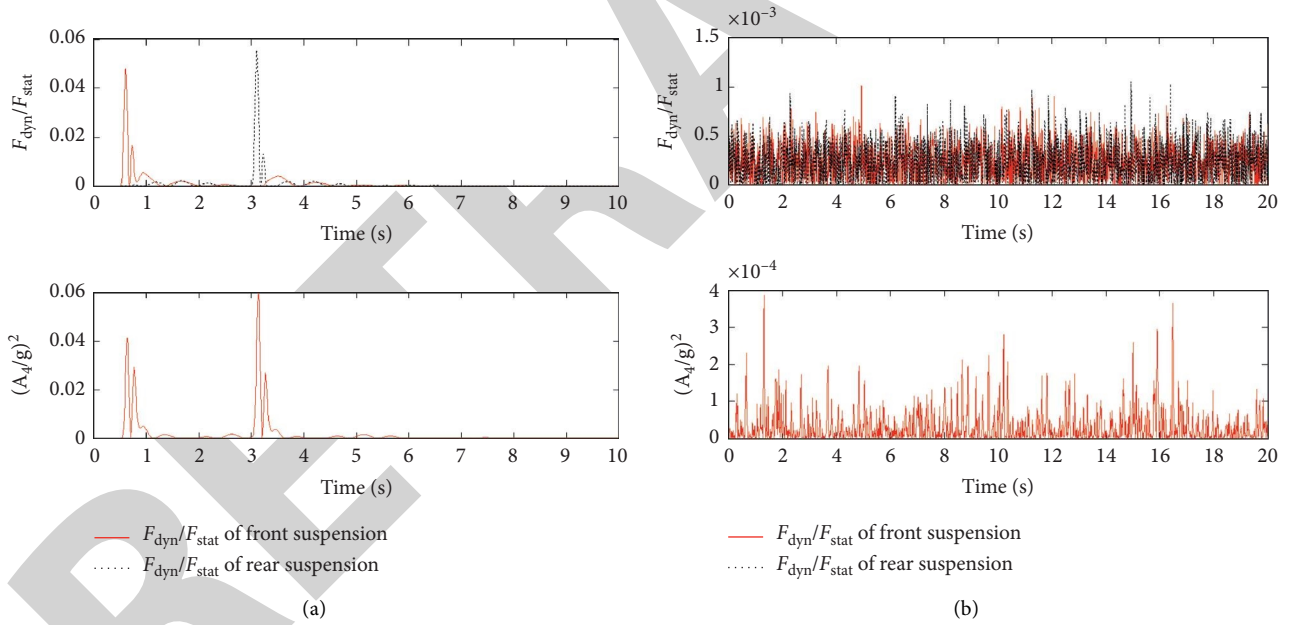


FIGURE 10: Responses of the ratio of dynamic loads and static loads of the front and rear tire against road inputs and the square of ratio of acceleration and gravity acceleration against the road inputs (a) for bump excitation and (b) for random inputs. The vehicle velocity  $v = 1.1256$  m/s (the time delay  $\tau = 2.5$  second), the simulation period  $T = 20$  seconds, and sampling interval  $(h) = 0.01$  seconds.

TABLE 3: Comparison of simulation response.

Items	Half vehicle system coupling with HNES model (this paper)		The model in the reference [23]		Vehicle velocity and time delay	
	Bump road inputs	Random road inputs	Bump road inputs	Random road inputs	$v$	$\tau$
$U_4$	0.032 m	$2.1e^{-3}$ m	0.04 m	0.038 m	1.1256 m/s	$\tau = 2.5$ s
$U_3$	0.022 rad	$1.78e^{-3}$ rad	0.03 rad	0.04 rad		
$A_4$	—	$0.152$ m/s <sup>2</sup>	—	$4.2$ m/s <sup>2</sup>		
$A_3$	—	$0.089$ rad/s <sup>2</sup>	—	$0.5$ rad/s <sup>2</sup>		

TABLE 4: Comparison of both ride comfort and drive safety.

Items	The model in the reference [23]		Half vehicle system coupling with the HNES model			
	Front suspension	Rear suspension	Front suspension	Rear suspension		
Ride	Bump inputs	2.28		3.7516e-5		
Comfort	Random inputs	4.6		2.0739e-4		
Drive	Bump inputs	1.34	1.96	5.3061e-5		2.5438e-5
Safety	Random inputs	5.32	4.31	3.8679e-4		2.5438e-5

parameters of the half vehicle system coupling with the HNES model have only been achieved for bump road inputs.

## 6. Conclusions

In this paper, the behavior and performance of a semi-active suspension consisting of the HNES for the half vehicle system has been proposed and investigated in shock mitigation. A successful validation process has been performed to solve the half vehicle system coupling with HNES using the same parameters to compare the developed model to the MR model. The response of the half vehicle system coupling with HNES is solved numerically using the direct time integration method (analog equation method). The model is simulated against two kinds of road inputs which are bump road inputs and random road inputs. The great performance of the model is evident as the velocity of the vehicle changes from 1.1256 m/s to 20 m/s. The main conclusions that can be drawn from this investigation are as follows:

- (i) The HNES model as a semiactive suspension coupled to the linear half vehicle system was studied

- (ii) The performance of semiactive suspension in half vehicle system coupling with the HNES model has a significant potential of reducing the road input disturbance

- (iii) The responses of displacements, velocities, and accelerations of the HENS model as a semiactive suspension in the half vehicle system are much better than those of the MR model as a semiactive suspension system for the same parameter in the time domain ( $v = 1.1256(\text{m/s})$ )

- (iv) The ride comfort and the drive safety of the HNES as a semiactive suspension in the half vehicle system both against the bump road inputs and random road inputs are much higher than those of the MR model given in the study [23]

## Appendix

### A. Matrices M, K, and C and Vectors F, Q, and U in equation (12)

Matrices M, K, and C and vectors F, Q, and U are

$$\mathbf{M} = \text{diag}(M_3, M_2, J, M_1, M_1, M_f, M_r),$$

$$\mathbf{K} = \begin{pmatrix} K_{f2} & -K_{f2} & K_{f2}L_3 & 0 & 0 & 0 & 0 & 0 \\ -K_{f2} & K_{f2} + K_{f2} + K_{NL} + K_r + K_{NL} & -K_{f2}L_3 - K_fL_1 - K_{NL}L_1 - K_rL_2 + K_{NL}L_2 & -K_{NL} & -K_f & -K_{NL} & -K_r & -K_r \\ K_{f2}L_3 & K_{f2}L_3 + K_fL_1 + K_{NL}L_1 + K_rL_2 + K_{NL}L_2 & K_{f2}L_3^2 - K_fL_1^2 - K_{NL}L_1^2 + K_rL_2^2 + K_{NL}L_2^2 & K_{NL}L_1 & -K_fL_1 & -K_{NL}L_2 & -K_rL_2 & -K_rL_2 \\ 0 & -K_{NL} & K_{NL}L_1 & K_{NL} + K_{EL} & -K_{EL} & 0 & 0 & 0 \\ 0 & -K_{NL} & -K_{NL}L_2 & K_{NL} + K_{EL} & -K_{EL} & K_{NL} + K_{EL} & -K_{EL} & -K_{EL} \\ 0 & -K_f & K_fL_1 & -K_{EL} & K_f + K_{EL} + K_{tf} & 0 & 0 & 0 \\ 0 & -K_r & -K_rL_2 & 0 & 0 & -K_{EL} & K_e + K_{EL} + K_{tr} & -K_{EL} \end{pmatrix},$$

$$\mathbf{C} = \begin{pmatrix} C_{f2} & -C_{f2} & C_{f2}L_3 & 0 & 0 & 0 & 0 & 0 \\ -C_{f2} & C_r + C_{f2} + C_f + 2C_2 & -C_{f2}L_3 - C_fL_1 - C_2L_1 + C_rL_2 + C_2L_2 & -C_2 & -C_f & -C_2 & -C_r & -C_r \\ -C_{f2}L_3 & C_{f2}L_3 + C_fL_1 + C_2L_1 + C_rL_2 + C_2L_2 & -C_{f2}L_3^2 - C_fL_1^2 - C_2L_1^2 + C_rL_2^2 + C_2L_2^2 & -C_2L_1 & -C_fL_1 & C_2L_2 & -C_rL_2 & -C_rL_2 \\ 0 & -C_2 & C_2L_1 & C_2 + C_1 & -C_1 & 0 & 0 & 0 \\ 0 & -C_2 & -C_2L_2 & 0 & 0 & C_2 + C_1 & -C_1 & -C_1 \\ 0 & -C_f & C_fL_1 & -C_1 & C_f + C_1 & 0 & 0 & 0 \\ 0 & -C_r & -C_rL_2 & 0 & 0 & -C_1 & C_r + C_1 & -C_1 \end{pmatrix},$$

$$\mathbf{F} = \begin{pmatrix} 0 & 0 & 0 & 0 \\ -F_{\text{BWf}} & -F_{\text{BWr}} & 0 & 0 \\ -F_{\text{BWf}} & -F_{\text{BWr}} & 0 & 0 \\ F_{\text{BWf}} & 0 & 0 & 0 \\ 0 & F_{\text{BWr}} & 0 & 0 \\ 0 & 0 & K_{\text{tf}} & 0 \\ 0 & 0 & 0 & K_{\text{tr}} \end{pmatrix}, \quad (\text{A.1})$$

$$\mathbf{Q} = (1 \ 1 \ q_1 \ q_2)^T,$$

$$\mathbf{U} = (U_5 \ U_4 \ U_3 \ U_{f2} \ U_{f1} \ U_{r2} \ U_{r1} \ U_{Zf} \ U_{Zr})^T.$$

## B. Probability Density and Distribution Function of Random Variable $\theta$

The probability density of random variable  $\theta$  is

$$f(\theta) = \begin{cases} \frac{1}{\pi - (-\pi)}, & -\pi < \theta < \pi, \\ 0, & \text{otherwise.} \end{cases} \quad (\text{B.1})$$

The distribution function of random variable  $\theta$  is

$$F(\theta) = \begin{cases} 0, & \theta < -\pi, \\ \frac{\theta - (-\pi)}{\pi - (-\pi)}, & -\pi \leq \theta < \pi, \\ 1, & \theta \geq \pi. \end{cases} \quad (\text{B.2})$$

## Data Availability

The data used to support the findings of this study are available from the corresponding author upon request.

## Conflicts of Interest

The authors declare that they have no conflicts of interest.

## Acknowledgments

This work was supported by the Key Research and Development Program of Gansu Province, China (Grant No. 18YF1GA063).

## References

- [1] P. Watts, "On a method of reducing the rolling of ships at sea. Read at the 24th Session of the Royal Institution of Naval Architects," Report no. 1883-12, RINA Transactions, Genova, Italy, 1883.
- [2] H. Frahm, *Device for Damping Vibrations of Bodies*, Google Patents, Dublin, Ireland, 1911.
- [3] B. Weber and G. Feltrin, "Assessment of long-term behavior of tuned mass dampers by system identification," *Engineering Structures*, vol. 32, no. 11, pp. 3670–3682, 2010.
- [4] M. A. AL-Shudeifat, "Highly efficient nonlinear energy sink," *Nonlinear Dynamics*, vol. 76, no. 4, pp. 1905–1920, 2014.
- [5] E. Boroson, S. Missoum, P.-O. Mattei, and C. Vergez, "Optimization under uncertainty of parallel nonlinear energy sinks," *Journal of Sound and Vibration*, vol. 394, pp. 451–464, 2017.
- [6] A. T. Savadkoohi, C.-H. Lamarque, and Z. Dimitrijevic, "Vibratory energy exchange between a linear and a non-smooth system in the presence of the gravity," *Nonlinear Dynamics*, vol. 70, no. 2, pp. 1473–1483, 2012.
- [7] M. Weiss, C. Mahmoud, S. Alireza Ture, and C. H. Lamarque, "Multi-scale energy exchanges between an elasto-plastic oscillator and a light nonsmooth system with external prestress," *Nonlinear Dynamics*, vol. 83, no. 1-2, pp. 109–135, 2016.
- [8] G. C. Tsiatas and A. E. Charalampakis, "A new hysteretic nonlinear energy sink (HNES)," *Communications in Nonlinear Science and Numerical Simulation*, vol. 60, pp. 1–11, 2018.
- [9] A. F. Vakakis and O. Gendelman, "Energy pumping in nonlinear mechanical oscillators: Part II-resonance capture," *Journal of Applied Mechanics*, vol. 68, no. 1, pp. 42–48, 2001.
- [10] O. Gendelman, L. I. Manevitch, A. F. Vakakis, and R. M'Closkey, "Energy pumping in nonlinear mechanical oscillators: Part I-dynamics of the underlying Hamiltonian systems," *Journal of Applied Mechanics*, vol. 68, no. 1, pp. 34–41, 2001.
- [11] A. T. Savadkoohi, C.-H. Lamarque, and M. V. Contessa, "Trapping vibratory energy of main linear structures by coupling light systems with geometrical and material nonlinearities," *International Journal of Non-linear Mechanics*, vol. 80, pp. 3–13, 2016.
- [12] D. Laxalde, F. Thouverez, and J.-J. Sinou, "Dynamics of a linear oscillator connected to a small strongly non-linear hysteretic absorber," *International Journal of Non-linear Mechanics*, vol. 41, no. 8, pp. 969–978, 2006.
- [13] J. T. Katsikadelis, "A new direct time integration method for the equations of motion in structural dynamics," *ZAMM - Journal of Applied Mathematics and Mechanics/Zeitschrift für Angewandte Mathematik und Mechanik*, vol. 94, no. 9, pp. 757–774, 2014.
- [14] J. T. Katsikadelis, "A new direct time integration method for the semi-discrete parabolic equations," *Engineering Analysis with Boundary Elements*, vol. 73, pp. 181–190, 2016.
- [15] R. Bouc, "Forced vibrations of mechanical systems with hysteresis," in *Proceedings of the Fourth Conference on Nonlinear Oscillations*, Prague, Czech Republic, September 1967.

- [16] Y.-K. Wen, "Method for random vibration of hysteretic systems," *Journal of the Engineering Mechanics Division*, vol. 102, no. 2, pp. 249–263, 1976.
- [17] A. Charalampakis and V. Koumousis, "On the response and dissipated energy of Bouc–Wen hysteretic model," *Journal of Sound and Vibration*, vol. 309, no. 3-5, pp. 887–895, 2008.
- [18] A. E. Charalampakis, "The response and dissipated energy of Bouc–Wen hysteretic model revisited," *Archive of Applied Mechanics*, vol. 85, no. 9-10, pp. 1209–1223, 2015.
- [19] G. Srijith and K. Jayaraj, "MR damper and its application in vehicle suspension system," *Mechatronics*, vol. 12, 2010.
- [20] J. Lin and D. Sun, "Application of pseudo excitation method to 3-D buffeting analysis of the Tsing Ma longspan suspension bridge," *Journal-Dalian University of Technology*, vol. 39, pp. 172–179, 1999.
- [21] International Organization for Standardization, *Mechanical Vibration and Shock–Evaluation of Human Exposure to Whole-Body Vibration–Part 5: Method for Evaluation of Vibration Containing Multiple Shocks*, International Organization for Standardization, Geneva, Switzerland, 2004.
- [22] L. Jiahao, "A fast CQC algorithm of PSD matrices for random seismic responses," *Computers & Structures*, vol. 44, no. 3, pp. 683–687, 1992.
- [23] M. Čorić, "Optimisation of active suspension control inputs for improved performance of active safety systems," *Vehicle System Dynamics*, vol. 56, no. 1, pp. 1–26, 2018.
- [24] M. A. Eltantawie, "Decentralized neuro-fuzzy control for half car with semi-active suspension system," *International Journal of Automotive Technology*, vol. 13, no. 3, pp. 423–431, 2012.